Available online at www.sciencedirect.com
SCIENCE DIRECT®
Computers and Structures 82 (2004) 653–658
Computers & Structures
www.elsevier.com/locate/compstruc

Temperature and stress fields induced during laser cladding

R. Jendrzejewski *, G. Śliwiński, M. Krawczuk, W. Ostachowicz

Institute of Fluid-Flow Machinery, Polish Academy of Sciences, Fiszera 14, 80-952 Gdańsk, Poland

Received 4 September 2003; accepted 25 November 2003

Abstract

For the laser cladding process the temperature and strain–stress fields were numerically calculated for the case of stellite SF6 coating on the X10Cr13 chromium steel. The effect of the base preheating on microcracking susceptibility of the coating was considered. A decrease of the strain stress generated in the coating from 1800 MPa for the non-preheated base (20 °C) to the value below the limit of the SF6 tensile strength of 900 MPa for the case with preheating (500 °C) was observed. For comparison with experiment the coatings were prepared by laser cladding with and without preheating of the base. Cracks were observed in photographs of the sample for the non-preheated case. Preheating at temperatures above 500 °C resulted in production of crack-free coatings, in agreement with the calculations.

Keywords: Temperature field; Strain–stress field; Laser cladding; Stellite coatings

1. Introduction

The laser cladding of metal powders for production of protective coatings of enhanced mechanical properties and also for repair of worn-out machine parts represents a cost-effective alternative to conventional techniques, such as plasma spraying, mechanical processing and moulding. In particular, the laser cladding of cobalt-based alloys (stellites, tribaloys) is of interest for the industrial applications, because these coatings exhibit a relatively high wear resistance, microhardness and a fine-grained, homogeneous microstructure [1–6].

It follows from the literature that the microcracking susceptibility of the laser-cladded layers represents a serious problem, which still limits a wider application of the considered technique [1,2]. In the extreme case the cracks may lead to disconnection of the coating from the base material. Recently, results of numerous investigations aimed at solving the problem were reported. The preheating of the substrate prior to the coating preparation is one of the widely discussed solutions [1,4,7]. However, the available data indicate that the modelling and description of the effects involved are quite complex due to laser interaction with a multiphase environment and fast melting of different materials (base and coating).

In this work the time-dependent temperature and stress fields developed during laser cladding are investigated in order to explain the cause of microcracking of the laser-cladded metallic coatings. The effect of base material preheating on the cracking susceptibility is taken into account. An efficient approach is proposed, allowing one to calculate numerically the thermal and strain–stress distributions. Results of calculations are compared with the experiment and discussed.

2. Formulation of the thermal and stress problems

The problem of the temperature distribution and the stress field was studied in connection with laser cladding realized by direct remelting of metal powders. The geometry of the laser beam—material interaction region is shown schematically in Fig. 1.

* Corresponding author. Tel.: +48-58-3411271; fax: +48-58-3416144.
E-mail address: rafj@imp.gda.pl (R. Jendrzejewski).

0045-7949/$ - see front matter © 2004 Elsevier Ltd. All rights reserved.
doi:10.1016/j.compstruc.2003.11.005

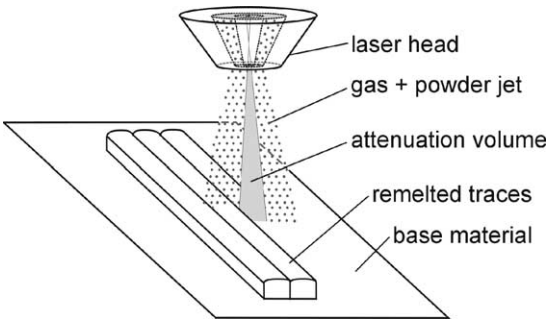

Fig. 1. Scheme of the one-step laser cladding of metal powders; the material is supplied co-axially with the laser beam.

The heat transfer processes: conductivity, convection, radiation and also the latent heat were taken into account. The input data required for numerical calculation by means of the ADINA code [8] were taken according to the experimental conditions, together with the respective values of the material constants characterizing the base plate and the metal powder to be melted. The base and the powder materials were the chromium steel X10Cr13 (13% Cr, 0.6% Ni, 0.6% Mn, 0.6% Si, 0.12% C, bal. Fe), and the Co-based stellite SF6 alloy (19% Cr, 13.5% Ni, 7.5% W, 3% Fe, 2.3% Si, 1.6% B, 1% Mn, 0.7% C, bal. Co), respectively. The thermal and strength properties of both materials are given in Table 1.

The other thermal and material properties of the steel and stellite were taken as follows:

- Young's modulus—206 GPa,
- Poisson's coefficient—0.3,
- convection coefficient—5 W/m^2 deg (at ambient temperature of 20 °C),
- Stefan–Boltzmann constant—5.7×10^{-8} (at 20 °C),
- emissivity coefficient—0.2.

The latent heat of X10Cr13 steel was estimated based on data available for materials of similar chemical composition. For Stellite SF6 the linear dependence of the conductivity and heat capacity on the temperature in the range 20–1120 °C was assumed and values corresponding to the interaction conditions were used—see Table 1.

The geometry of the interaction zone was defined by the base plate dimensions of 55 mm × 55 mm × 6 mm, and these of the coated material. The coating was located in the middle of the base surface. It consisted of 20 parallel paths 1 mm wide. The length and height of the paths were 20 mm × 0.2 mm. For the processing speed of the laser head (scanning speed) a constant value of 10 mm/s was assumed.

For numerical calculations the ADINA code (Ver. 7.5) was used. The time dependent temperature distribution was calculated using the ADINA-T code developed for the thermal field analysis. The problem of the strain–stress field was solved using the ADINA code. For the heat transfer by conduction in the base and coating material 20-node finite elements (3D conductive elements) were applied [9]. Those elements were described by quadratic shape functions. For modelling of the convection and radiation processes considered in the heat transfer analysis the "Boundary Convection" and "Boundary Radiation" elements with eight nodes were used.

Increase of the total mass of the solid material during the cladding process was taken into account in the numerical modelling, because a part of the powder material accumulated on the base plate surface in the form of a solid layer, resulting in a temporal dependence of the structure geometry. Accordingly, the "*Birth/Death*" option of the code was used in the numerical calculations. This option enabled a time-dependent activation and deactivation of the finite elements. It was used for the elements describing the melted powder material, and for the elements applied in modelling of the convection and radiation on the base surface as well. The "*Birth/Death*" option was used for description of new-formed fragments of the build-up. The scheme described above enabled changes of the configuration in arbitrarily selected time instants.

The energy supplied by the moving laser head was modelled by a code option called *distributed heat flux*. It enabled us to define the position of the laser head for individually defined time functions. The initial thermal fields of a given specimen were modelled by the option *prescribed temperature*. This enabled assuming arbitrarily chosen temperatures for selected regions.

In the numerical calculations the relation between the temperature and material parameters was taken into

Table 1
Thermophysical properties of X10Cr13 steel and stellite SF6 alloy powder

	Density (kg/m^3)	Latent heat (J/kg)	Melting temperature (°C)	Linear expansion coefficient (1/deg)	Tensile strength (MPa)	Conductivity (W/m deg)	Heat capacity (J/kg deg)
X10Cr13 steel	7800	272,000[a]	1460	10.5×10^{-6}	680	29.3	460
Stellite SF6	8400	310,000	1350	17.4×10^{-6}	1020	14–45	426–801

[a] Estimated value.

account. Also thermal effects associated with the change of the material phase, i.e. the *latent heat* were taken into consideration.

Due to the non-linearity of the above described problem the equations of motion were solved by back integration, using the Euler scheme together with the Newton–Raphson iterative procedure. 400 incremental time steps with $\Delta t = 0.1$ s each were used. For each step the program realized 30 iterations. The discrete model was described by 2200 equations.

Results of the calculations were obtained in the form of time-dependent temperature distributions. They were used next in the calculations for the stress–strain problem. In this case the materials of the base and cladded paths were modelled by 20-node finite elements with three translational degrees of freedom per node. The cladding process was modelled by the aid of the "*Birth/Death*" option. This option was adopted for all the considered finite elements, just as in the ADINA-T code. The thermal fields were used as loads in the consecutive time steps. It was assumed that the bottom surface of the plate was fixed.

The numerical model considered had 6600 degrees of freedom. The problem was numerically solved on a PC (Celeron 400 MHz processor). The calculation time did not exceed 1800 s.

3. Results of calculations

The time-dependent temperature and stress were calculated at arbitrarily chosen points of the discrete model P_i and E_i, respectively, for the initial base temperature of 20 and 500 °C, i.e. for a non-preheated and preheated case. A scheme showing locations of these points and elements together with the reversal movement trajectory of the laser head is given in Fig. 2. Points P are placed in the middle of the appropriate elements, whereas points E are situated in the middle of the bottom surface of these elements—see the right part of Fig. 2. It should be pointed out that the diagrams of the temporal dependences are related to the respective points P_i and start from the points they concern, because the considered points (P1–P4) come into being during the laser beam passage through these locations. On the other hand, the stress diagrams begin at a time $t = 0$, as the bottom surface of the coating elements is just the same as the upper surface of the base elements.

Results of calculations are shown in Figs. 3–5. The first temperature and stress peaks shown in Fig. 3 correspond to the laser beam passage across the element in which points P1 and E1 are located. The consecutive peaks are generated as a result of the heat transfer from the laser beam passing along adjacent traces. The time difference between the first and second peaks is equal to about 4 s, which coincides with the distance of 40 mm

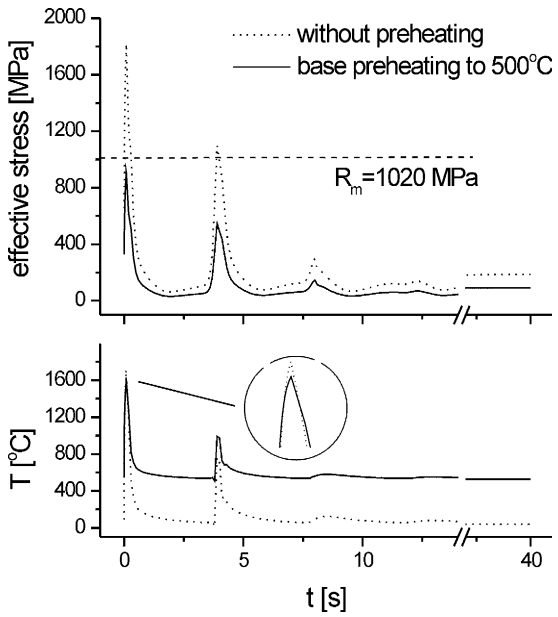

Fig. 3. The time dependences of the temperature (point P1) and reduced stress (point E1) for the base initial temperatures of 20 °C (dots) and 500 °C (solid line).

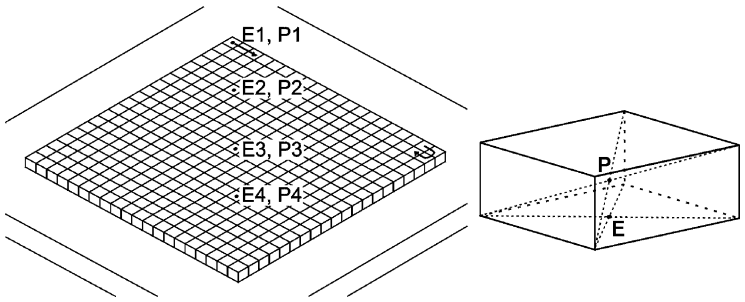

Fig. 2. A discrete model of the laser–material interaction zone. A view of the build-up 40 s after starting the process, and points selected for presentation of the calculation results.

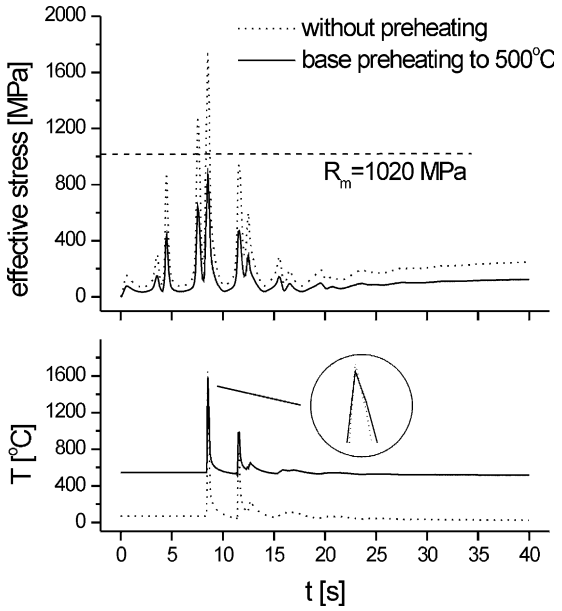

Fig. 4. The temporal changes of the temperature (P2) and reduced stress (E2) calculated for the base initial temperatures of 20 °C (dots) and 500 °C (solid line).

passed by the laser beam at the scanning speed of 10 mm/s. The laser beam is then crossing the next element—the last in the second trace. The heights of the first temperature peaks for both considered cases, i.e. for the preheated and non-preheated base, exceed 1500 °C. This indicates that the condition of melting of both the coating and base materials is fulfilled, and a proper bonding between them can be obtained. The effective stress diagram reveals two marked peaks, which temporally coincide with temperature peaks. The value of tension induced in the coating made without preheating exceeds the value of the tensile strength of stellite. Therefore microcracks are expected in that case. This is evident from the observation of the first and second peaks of the dotted line in the upper part of Fig. 3. On the other hand, the reduced stresses shown for point E1 in the case of cladding on a preheated base material do not exceed 900 MPa. That value is smaller than the limit of tensile strength of the investigated stellite. In this case microcracks should not appear in the cladded material.

The first temperature peak illustrated in Fig. 4 corresponds to the laser beam passage through the element containing point P2. The temperature exceeds 1500 °C and this assures melting of both materials. Other peaks appear as an effect of the thermal field generated by the laser beam passage of the neighbouring points. The upper diagram illustrates the effective stress changes. Several peaks are revealed. The highest peaks in dotted and solid lines correspond to the laser head passages across the element including point E2. Other peaks

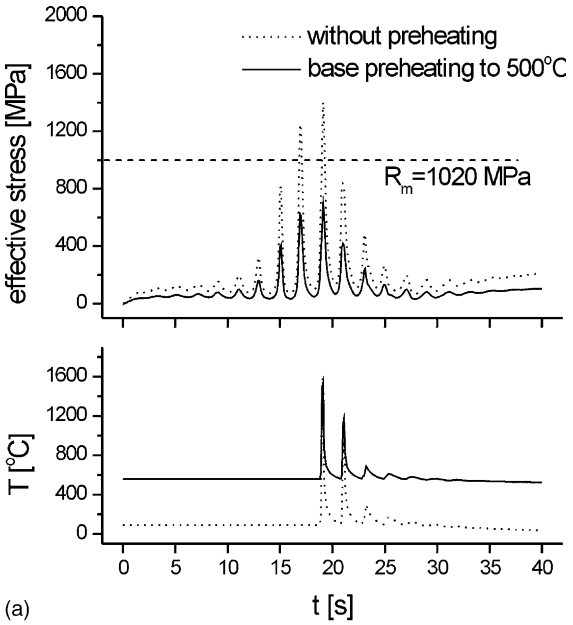

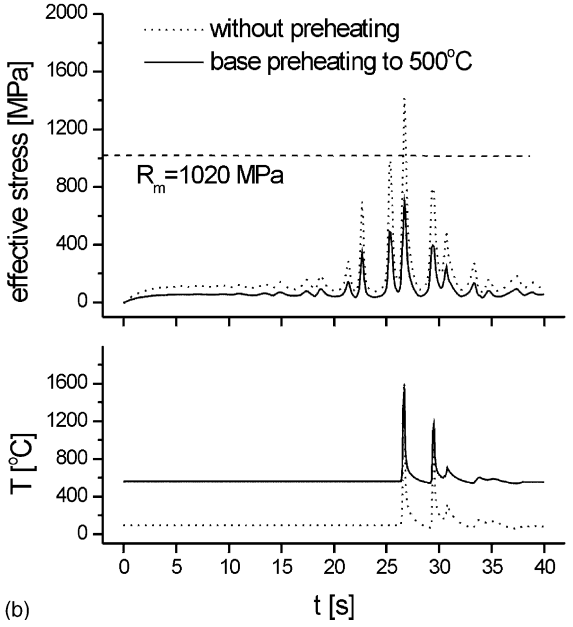

Fig. 5. The time dependences of the temperature and reduced stress at P3 and E3 (a), and at P4 and E4 (b) respectively, for the base preheating temperatures of 20 °C (dots) and 500 °C (solid line).

correspond to the beam passage along the paths located close to this element. Values of stresses induced in the sample made on the non-preheated base exceed the value of the stellite tension strength, both during the beam passage through the considered element and along paths located close to this element. Therefore microcracks are

expected in this element, while the maximum stress in the coating on the preheated base reaches 880 MPa, which is below the tensile strength limit for the melted material.

A similar decrease of the effective stress in the coatings on a preheated substrate was observed for the following points, and the example diagrams for two of them are presented in Fig. 5. It is worth noting that the maximal values of stresses in the middle of the coating, i.e. about 1400 MPa (non-preheated base) and 700 MPa (preheating applied) for points E3 and E4 are smaller than those calculated for points E1 or E2 close to the coating border (about 1800 and 900 MPa in the non-preheated and preheated case, respectively). This means that the coating borders located close to the starting point of the process reveal a higher cracking susceptibility. This is due to the larger temperature gradients in the initial stage of the cladding process. Moreover, according to the results shown in Fig. 5 the areas near points P1 and P2 are almost not affected by the laser beam passage across points P3 and P4. This conclusion is based on the fact that after about 15 s the change of the effective stress is negligible. The above consideration indicates that conclusions regarding the cracking susceptibility at the chosen locations can be correct even for coatings of larger dimensions than those modelled here.

In contrast to the stress data, the values of the corresponding temperature peaks are comparable to each other, despite different initial temperatures of the base material. This result is due to the reduced value of the laser beam flux applied for calculation of the case with preheating.

4. Comparison with experiment

In order to check the correctness of the model assumptions and the calculated results, experimental investigations were carried out. Samples of coatings were produced by means of a 1.5 kW cw CO_2 laser equipped with a numerically controlled XYZ manipulator. Positioning and feeding of the samples were ensured by a processing table. During the process, the powder material was delivered into the processing zone in a stream of carrier gas (Ar) by means of a multi-stream nozzle, as shown diagrammatically in Fig. 1. Two additional Ar streams were applied for shielding of the focusing optics and preventing production of oxides and contaminations. The laser stand has been described in detail elsewhere [2,6].

For the coatings the stellite SF6 powder, characterized by grains of spherical shape and diameter of about 60 μm was used. 6 mm-thick plates of X10Cr13 steel with a composition similar to that used for steam turbine blades were used as substrates. The single trace width was equal to about 1 mm and the laser beam scanning speed relative to the base material was kept at 10 mm/s. Coatings of 2×2 cm^2 area and thickness in the range from 0.15 to 0.3 mm, depending on the powder feed rate, were produced. The sample and modelled coatings had equal volumes.

The samples were prepared with and without preheating of the base material. Preheating temperatures in the range from 450 to 600 °C were applied prior to the laser cladding in order to diminish or eliminate crack development in the deposited coatings. The temperature of the heated base material was controlled by means of a Kleiber 270B fast infrared pyrometer (15 μs response time).

Two constant laser irradiation levels of 1100 and 800 W were adopted for production of coatings on the cold and preheated bases. The laser beam was focused by means of a lens optics (ZnSe, $f = 127$ mm) into a spot of about 0.3 mm at the nozzle outlet, while on the base material, placed 7 mm below the focal point, a constant diameter of 1 mm was maintained. This resulted in changes of the beam intensities between the nozzle and the substrate from 8.6×10^5 to 9.4×10^4 W/cm^2 for the laser beam power $P = 800$ W, and from 1.2×10^6 to 1.3×10^5 W/cm^2 for $P = 1100$ W. Powder melting occurred at intensities between these limits, whereas values

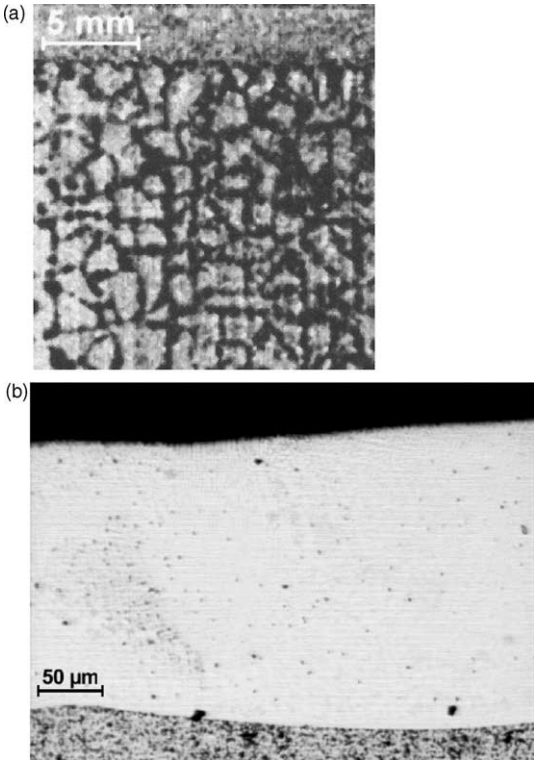

Fig. 6. A cracked stellite coating on the non-preheated base material (a), and a crack-free cross-section obtained on the base material preheated at 500 °C (b).

on the base surface were lower, but sufficient to melt the substrate and fuse it with the impinging coating particles. The values of the laser beam intensities used for powder melting, multiplied by the absorption coefficient of 11% taken from the literature [10], corresponded to the heat flux values assumed for modelling.

The experimental results were compared with the calculated data. An inspection of the sample surface and cross-sections was performed by means of the optical and scanning electron (SEM) microscopes. Fig. 6a shows cracks in the coating cladded on the cold base i.e. without preheating. The cracking susceptibility was evidenced in all samples processed under the conditions mentioned. However, it was found that the number of cracks decreased with an increase of the base preheating temperature and the crack-free coatings were obtained for temperatures starting from about 480 °C—see example on Fig. 6b. The extended SEM revealed a well remelted, dendritic structure of the stellite coating, characterized by a metallurgical bond between the substrate and the laser remelted material. This experimental result confirms the conclusion from the temperature fields calculations, where maximal temperatures exceeding the melting point of both substrate and stellite materials were evidenced.

5. Conclusions

Numerical calculations of the time-dependent temperature and stress fields induced during laser cladding were performed. For the thermal and stress problems a discrete model was applied and the solutions were obtained by means of ADINA code with a implemented finite element module.

Results of calculations indicate that an initial heating of the base material contributes significantly to the decrease of stresses generated in the coating. The maximum calculated stress for an assumed initial base temperature of 20 °C reached 1800 MPa, exceeding thus the limit of the stellite SF6 tensile strength of 900 MPa. This indicated a possible occurrence of microcracking.

The stress values calculated for the initial base temperature of 500 °C were lower than the mentioned limit and allowed one to expect crack-free coatings. Moreover, the results showed that in order to get the desirable technological effect of the laser cladding with the base preheating applied, the laser beam intensity should be significantly lower (by about 60%) compared to the case without preheating.

Experimental verification of the numerical results was made. Sample coatings of stellite SF6 were prepared by laser cladding with and without preheating of the chromium steel base. In the photographs of the sample surface and cross-section cracks in the coating prepared on a cold substrate were observed. With increase of the temperature of base preheating decrease of the number of cracks was observed. Preheating at temperatures above 500 °C resulted in production of crack-free coatings.

The numerical model used and solutions obtained gave a valuable insight into laser cladding and valuable solution data as evidenced by the comparison with the experimental results. Results of the calculations will be applied in the pre-selection of parameters for the laser cladding process in the forthcoming work.

Acknowledgement

This work was sponsored by the State Committee for Scientific Research (KBN) under contract no. 0809/T08/02/22.

References

[1] Vilar R. Laser alloying and laser cladding. Mater Sci Forum 1999;301:229–52.
[2] Jendrzejewski R, Conde A, de Damborenea J, Śliwiński G. Characterisation of the laser-clad stellite layers for protective coatings. Mater Design 2002;23:83–8.
[3] Kathuria YP. Some aspects of laser surface-cladding in the turbine industry. Surf Coatings Technol 2000;132:262–9.
[4] Przybyłowicz J, Kusiński J. Laser cladding and erosive wear of Co–Mo–Cr–Si coatings. Surf Coatings Technol 2000;125:13–8.
[5] Sexton L, Lavin S, Byrne G, Kennedy A. Laser cladding of aerospace materials. J Mater Process Technol 2002;122:63–8.
[6] Jendrzejewski R, Conde A, de Damborenea J, Śliwiński G. Experimental study of a laser processing head with integrated jet of metal powder for rapid prototyping and production of protective coatings. Proc SPIE 2000;4184:603–6.
[7] Choi J, Mazumder J. Synthesis of Fe–Cr–C–W using laser cladding technique. J Mater Sci 1994;29(17):4460–76.
[8] ADINA—Theory and Modelling Guide, vol. I. Report ARD 00-7, Watertown, USA, August 2000.
[9] Bathe KJ. Finite elements procedures. Englewood Cliffs, NJ: Prentice-Hall; 1996.
[10] Frenk A, Vandyoussefi M, Wagniere JD, Zryd A, Kurz W. Analysis of the laser cladding process for stellite on steel. Metall Mater Trans 1997;28B:501–8.